AGU PUBLICATIONS

Geophysical Research Letters

RESEARCH LETTER
10.1002/2014GL059348

Key Points:
- There is a better agreement between observation and modeling
- The density stratification affects only traveltime
- The elastic loading affects traveltime and changes the wave form

Supporting Information:
- Readme
- Figure S1
- Figure S2

Correspondence to:
S. Allgeyer,
sebastien.allgeyer@anu.edu.au

Citation:
Allgeyer, S., and P. Cummins (2014), Numerical tsunami simulation including elastic loading and seawater density stratification, *Geophys. Res. Lett.*, *41*, 2368–2375, doi:10.1002/2014GL059348.

Received 26 JAN 2014
Accepted 24 MAR 2014
Accepted article online 27 MAR 2014
Published online 11 APR 2014

Numerical tsunami simulation including elastic loading and seawater density stratification

Sébastien Allgeyer[1] and Phil Cummins[1]

[1]Research School of Earth Sciences, Australian National University, Canberra, ACT, Australia

Abstract Systemic discrepancies between observed and modeled tsunami wave speeds were previously identified for two recent major tsunamis: the 2010 Maule and 2011 Tohoku events. To account for these discrepancies, we developed a numerical tsunami propagation code solving the shallow water equation and including the effects of elastic loading of the seafloor by the tsunami as well as a linear density profile in the seawater column. We show here that both effects are important to explain the commonly observed difference between observations and simulations. We conclude that the density variation in the seawater column affects the wave speed without changing the waveform, whereas the loading effect has an effect on the wave speed and the waveform showing a negative phase before the main arrival due to the depression of the seafloor surrounding the tsunami wave. The combination of both effects is needed to achieve a better match between observations and simulations.

1. Introduction

Tsunami waveforms are fundamental data used to study the source mechanisms of large submarine earthquakes and the mechanism by which they generate tsunamis. Many studies have modeled the waveforms of tsunamis generated by such earthquakes using the shallow water theory that describes waves having wavelengths much longer than water depth over a rigid ocean floor. However, it has been known for some time that the solid Earth deforms in response to the surface load of the tsunami water mass, and this deformation has been observed in several studies [*Nawa et al.*, 2007; *Okal*, 2007; *Boudin et al.*, 2013].

Recent high-quality observations of the tsunamis generated by the 2010 Maule and 2011 Tohoku-Oki earthquakes on offshore deep-ocean pressure sensors have established conclusively that there are significant discrepancies between the observed waveforms and those computed using standard shallow water theory. These discrepancies mainly take the form of a delay in the time of arrival and a small drawdown prior to the first-arriving positive peak in the waveform for the observed versus computed waveforms [e.g., see *Fujii and Satake*, 2012, Figure 2; *Grilli et al.*, 2012, Figure 14].

While in the past apparently minor discrepancies in tsunami traveltime were often attributed to factors such as error in the bathymetry [e.g., *Baba et al.*, 2009], numerical truncation, in the sphericity derivation [e.g., *Kirby et al.*, 2013]; the observations from the 2010 Maule and 2011 Tohoku events show that these errors are significant and systematic, especially in the far field. These observations prompted recent studies [*Tsai et al.*, 2013; *Watada*, 2013] that used simplified models of the coupled ocean-solid Earth system to argue that the observed discrepancies are mainly due to two effects not included in the standard shallow water theory: (1) elastic loading of the solid Earth by the tsunami and (2) compressibility of the seawater. These studies showed these effects can reduce tsunami speeds by 1–2%, resulting in delays of more than 10 min in transoceanic paths of the type of long-wavelength tsunami generated by the 2010 Maule and 2011 Tohoku events, which excludes a major contribution of Boussinesq-type dispersion, acting on short wavelength.

Tsai et al. [2013] advocate correcting for the tsunami arrival time by using their predictions for a flat Earth of uniform ocean depth. *Inazu and Saito* [2013] consider a more complete accounting of the surface loading effect in an ocean of variable depth by effectively adjusting the velocity term in the shallow water equations. However, this last approach does not account for the change in waveform of the tsunami due to the dispersion inherent to the surface loading effect, and in particular, it fails to account for the drawdown often observed prior to the first positive peak in many of the tsunami observations. The approach of *Tsai et al.* [2013] could potentially account for such effects in the direct wave by applying corrections separately to each frequency.

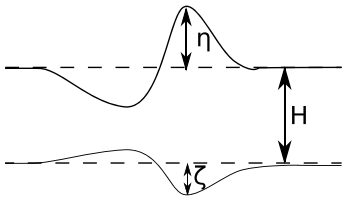

Figure 1. Schematic illustration of the tsunami loading effect. In this new model, the variation in ocean mass due to the tsunami causes elastic deformation of the seafloor.

In this paper we show how a more rigorous approach can take the surface loading and stratification effects into account in realistic tsunami simulations. We modify the standard shallow water equations to include the response of the ocean floor due to the excess tsunami wave mass loading and a linear seawater density profile. Although computationally expensive, comparisons of tsunami loading calculations using seismic source models of the Maule 2010 and Tohoku 2011 earthquakes show that it can reproduce most of the delay in apparent arrival time and also the waveform distortion evident in recent high-quality observations of deep-ocean tsunamis.

2. Description of the Model

The computation of tsunami propagation in the deep ocean on a rigid substrate is usually based on the shallow water, nondispersive approximation to the hydrodynamic (Navier-Stokes) equations. In the most general case, these equations are divided into a set of two hyperbolic equations, expressing the conservation of momentum and mass, respectively:

$$\frac{\partial \vec{u}}{\partial t} + (\vec{u} \cdot \vec{\nabla})\vec{u} = -g\nabla\eta + \vec{f}, \tag{1}$$

$$\frac{\partial \eta}{\partial t} + \nabla \cdot [\vec{u}(H+\eta)] = 0. \tag{2}$$

Here $\vec{u}$ denotes the horizontal component of the velocity integrated over the water column, η is the variation of sea level, from a reference level of 0 for an ocean at rest, and $\vec{f}$ normally represents the Coriolis and bottom friction. (For the deep-ocean simulations presented here bottom friction is regarded as negligible.). H is the depth of the ocean at rest so that the total water depth is $D = \eta + H$.

Following *Hendershott* [1972] (equation (3)), the motion of the seabed is accounted for by modifying the continuity equation as follows:

$$\frac{\partial(\eta+\xi)}{\partial t} + \nabla \cdot [\vec{u}(H+\eta)] = 0 \tag{3}$$

where ξ is the displacement of the seabed from it's depth H when at rest (measured downward, see Figure 1). Note that while the exact expression for total water depth is $D = H + \eta + \xi$, in equation (3) we use $D \approx H + \eta$, since as we argue below $|\nabla\xi| \ll |\nabla\eta|$.

To account for the density stratification of seawater, we follow *Tsai et al.* [2013] in using a linear approximation of the density profile,

$$\rho(z') = \rho_0(1 + \rho_0 g(H + \eta - z')/\kappa), \tag{4}$$

where κ is the bulk modulus of seawater and ρ_0 is the surface density. Analogously to the 1-D case considered by *Tsai et al.* [2013], we obtain the depth-averaged continuity equation as

$$\rho_H \frac{\partial(\eta+\xi)}{\partial t} + \rho_{\text{avg}} \nabla \cdot [\vec{u}(H+\eta)] = 0, \tag{5}$$

where $\rho_H \approx \rho_0(1 + \rho_0 gH/\kappa)$ is the density at the ocean floor and $\rho_{\text{avg}} \approx \rho_0(1 + \rho_0 gH/(2\kappa))$ is the average density, where we have assumed $\eta \ll H$.

As described below, synthetic tsunami waveforms are calculated using a finite difference implementation of equation (1), together with equations (2) and (5) for the case with and without surface loading, respectively. A Sommerfield radiation condition is realized at the open boundaries of the computational domain:

$$\frac{\partial(\eta+H)}{\partial t} - c\frac{\partial(\eta+H)}{\partial x} = 0, \tag{6}$$

where c is the nondispersive wave velocity of the tsunami ($\sqrt{g \cdot H}$). A Neuman boundary equation,

$$\vec{u} \cdot \vec{n} = 0, \tag{7}$$

is used for the wet-dry boundary (i.e., total reflection). In other words, no inundation is computed in this study.

3. Incorporation of Elastic Loading

The Earth's response to a mass loading its surface can be calculated using a Green's function that describes the response to a unit mass load concentrated at a point on its surface. *Longman* [1962] has shown that such a Green's function can be expressed as a sum over spherical harmonics of the form:

$$G(\mathbf{r}', \mathbf{r}) = G(\alpha) = \frac{a}{M_e} \sum_{n=0}^{\infty} h'_n P_n(\cos\alpha) \tag{8}$$

where $\mathbf{r}$ denotes a position on the Earth's surface with the point mass located at $\mathbf{r}'$, P_n refers to the nth Legendre polynomial, α the angular distance between $\mathbf{r}'$ and $\mathbf{r}$, a is the Earth radius and M_e is the mass of the Earth, and h'_n is the loading Love number of angular order n. The h'_n can be calculated for any radially symmetric Earth model, and results for $G(\alpha)$ are tabulated in, e.g., *Pagiatakis* [1990] and *Farrell* [1972].

As shown by *Hendershott* [1972], the seabed displacement term ξ in equation (3) can be calculated by convolving the Green's function with the change in ocean depth $\eta + \xi$:

$$\begin{aligned}\xi(\mathbf{r}) &= \int_S G(\mathbf{r}', \mathbf{r})[\eta(\mathbf{r}') + \xi(\mathbf{r}')]\mathrm{d}S \\ &= a\int_0^{2\pi}\int_0^{\pi} G(\alpha)[\eta(\alpha,\beta) + \xi(\alpha,\beta)]\cos(\alpha)\,\mathrm{d}\alpha\,\mathrm{d}\beta \\ &\approx a\int_0^{2\pi}\int_0^{\Delta\alpha} G(\alpha)\eta(\alpha,\beta)\cos(\alpha)\,\mathrm{d}\alpha\,\mathrm{d}\beta\end{aligned} \tag{9}$$

where S is the Earth's surface and α and β are colatitude and longitude, respectively, in a coordinate system with $\mathbf{r}$ as origin. Note the last line in equation (9) has made two approximations: (1) $\eta + \xi$ has been replaced by η, since $|\xi| \ll |\eta|$ and (2) the integral over α has been truncated at a distance $\Delta\alpha$, since the point source Green's function rapidly decays in magnitude with distance from the origin. We have tested this latter approximation to the convolution integral and found that a value of $\Delta\alpha = 800$ km is adequate for the calculations presented here, although, in general, the choice of $\Delta\alpha$ might depend on the tsunami wavelength.

4. Numerical Method

The shallow water equations (equations (1) and (2)/(3)/(5)) are solved over a staggered grid (Arakawa C-grid [*Arakawa and Lamb*, 1977]), with the velocities computed at the midpoints of the cell boundaries and the tsunami surface heights computed in the middle of the cell. The time stepping that we use is a semiimplicit *Crank and Nicolson* [1947] numerical scheme to ensure stability.

The computational method for including the surface loading effect follows the following steps. Starting from a time step n with the different variables η^n, u^n, v^n, and ξ^n.

1. The classical shallow water equations with rigid substrate and vertical density profile are solved. This gives us the first approximation of the surface and velocity field at the time $n + 1$ (η^*, u^*, v^*)
2. The bottom deformation ξ^{n+1} is computed by the convolution of the mass distribution from the surface η^* with the Green function (equation (9)). (This is step accounts for about 70% of the computation time.).
3. The value of η^* is corrected by the appropriate equation (see equation (5)) to give the final values at the $n + 1$ time step: η^{n+1}.

5. Earthquake Source Models

In order to compare our numerical results for tsunami including loading and stratification with observations, we consider initial sea level conditions that are appropriate for the 2010 Maule and 2011 Tohoku earthquakes. Since these earthquakes have been studied extensively, there are many source models that could be used. Here we consider the models of *Lorito et al.* [2011] and *Lay et al.* [2010] and *Satake et al.* [2013] and *Ammon et al.* [2011] for the 2010 Maule and 2011 Tohoku events, respectively.

The sea level displacement we use as the initial condition for tsunami simulation is taken to be equal to the combined effect of vertical and horizontal seafloor displacement on the vertical displacement of the water column on the same 2′ grid used for the computations, and bathymetry is from the 30" GEBCO grid

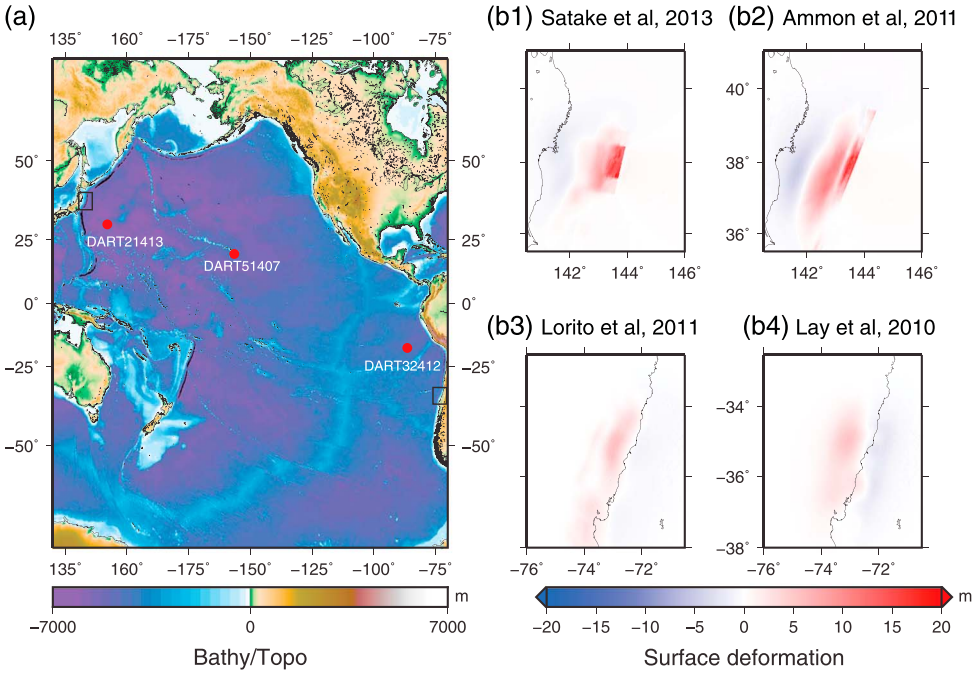

Figure 2. (a) The geographic domain and location of the DART sensors used in this study, with source areas indicated by rectangles. (b) The different initial surface of deformation models used for the Tohoku tsunami ((b1) *Satake et al.* [2013] and (b2) *Ammon et al.* [2011]) and the Maule tsunami ((b3) *Lorito et al.* [2011] and (b4) *Lay et al.* [2010]).

[*IOC et al.*, 2003] (see Figure 2a for the geographic location and Figures 2b1–2b4 for the source models). The seafloor displacement computed for each earthquake slip model is based on analytic formulae for a dislocation in a homogeneous half-space, as implemented by *Okada* [1985].

The source models of *Lorito et al.* [2011] and *Satake et al.* [2013] were obtained by inverting observed tsunami waveforms, but they may be biased because these studies did not account for tsunami self-loading or seawater density stratification. The models of *Lay et al.* [2010] and *Ammon et al.* [2011] were obtained by inverting seismic waveforms and are therefore not likely affected by such a bias. In any case, a comparison of the earthquake source models for each event (i.e., Figure 2b1 versus Figure 2b2 and Figure 2b3 versus Figure 2b4) shows substantial differences over length scales of 50–100 km, corresponding to tsunami arrival time differences of 5–10 min. Therefore, if we want to resolve such differences using tsunami data, we need to model the arrival times to a better accuracy than this. Due to the high shallow slip for the Tohoku earthquake source, which generates a very sharp peak in the surface deformation, we used a Gaussian filter of 40 km of radius to smooth the initial surface; one of the effects of using the filter could be a slight underestimate of the tsunami amplitude.

6. Results

We compare our results computed for the earthquake models in Figure 2b to the tsunami waveforms recorded by the three ocean-bottom pressure (DART) sensors shown in Figure 2a. We run our new tsunami code for two cases, with and without the loading and density stratification effects. Figure 3 shows the comparison of the observed tsunami waveforms with the simulated deep-ocean records at the three locations for both events, using the seismic derivative sources (in red) and the tsunami derivative sources (in blue). We compare the simulations to the de-tided deep-ocean observation. No filtering was applied on either the observed or simulated waveforms, apart from a vertical shift applied to the observed data to align it with a zero reference level prior to the tsunami arrival.

For sensors close to the sources (Figures 3a and 3f), the effect of the loading/stratification is small. The effects of loading and density stratification vary with distance as can be seen in Figures 3b and 3c and in Figures 3d and 3e for the 2010 Maule and 2011 Tohoku events, respectively. For these observations the sim-

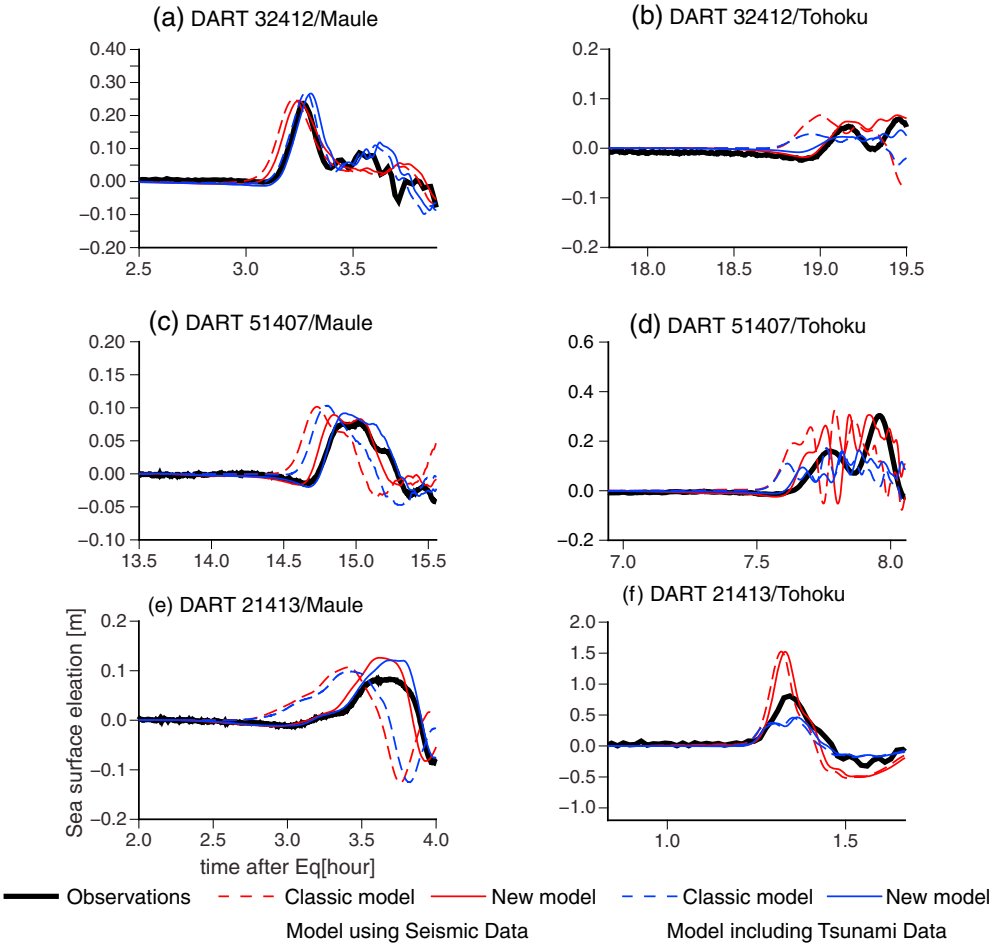

Figure 3. Comparison between observation and simulation for the two events in three different locations. In black are observations (No filter was applied, but the traces were shifted vertically shift to correspond to zero sea level prior to the arrival of the tsunami.), in red the simulation with the sources derived from seismic data (*Lay et al.* [2010] and *Ammon et al.*, [2011] for the Maule and Tohoku-Oki event, respectively), and in blue the simulations for sources based on tsunami data (*Lorito et al.* [2011] and [*Satake et al.* 2013]). The dashed curves represent the classical tsunami simulation, and the solid curves represent the simulations using the loading and stratification effect.

ulations that include loading and density stratification result in a better agreement between simulation and observation as well as a better fit in the first negative phase observed before the main wave.

Figure 4 shows a snapshot of the tsunami height after 14 h of propagation. The first negative phase is clearly observable for both events.

In order to show the different contributions of the loading and density stratification effects on the waveform, we solve the shallow water equations by adding each effect separately. Figure 5 shows the simulated time series on the DART51407 for the Maule tsunami. In agreement with *Tsai et al.* [2013], we conclude that the density stratification results only in a time delay and does not otherwise distort the waveform. The surface loading, on the other hand, not only changes the time of the (positive) peak arrival but also distorts the waveform, which can be seen in Figure 5 by the emergence of a long-period, negative peak prior to the positive peak of the main arrival. This negative phase is the result of the loading effect and is due to the downward flexure of the seafloor in response to the weight of the tsunami.

Plots of similar waveform comparisons for all the available DART data for the events studied are shown in Figures S1 and S2 in the supporting information. For all of the DART waveforms, our new calculations provide a better fit to the observations than calculations using standard shallow water theory. There remains significant misfit, however, and we speculate that this may be due to any combination of the following reasons: (1) errors in bathymetry, (2) errors in the source models, (3) a longer effective wavelength for

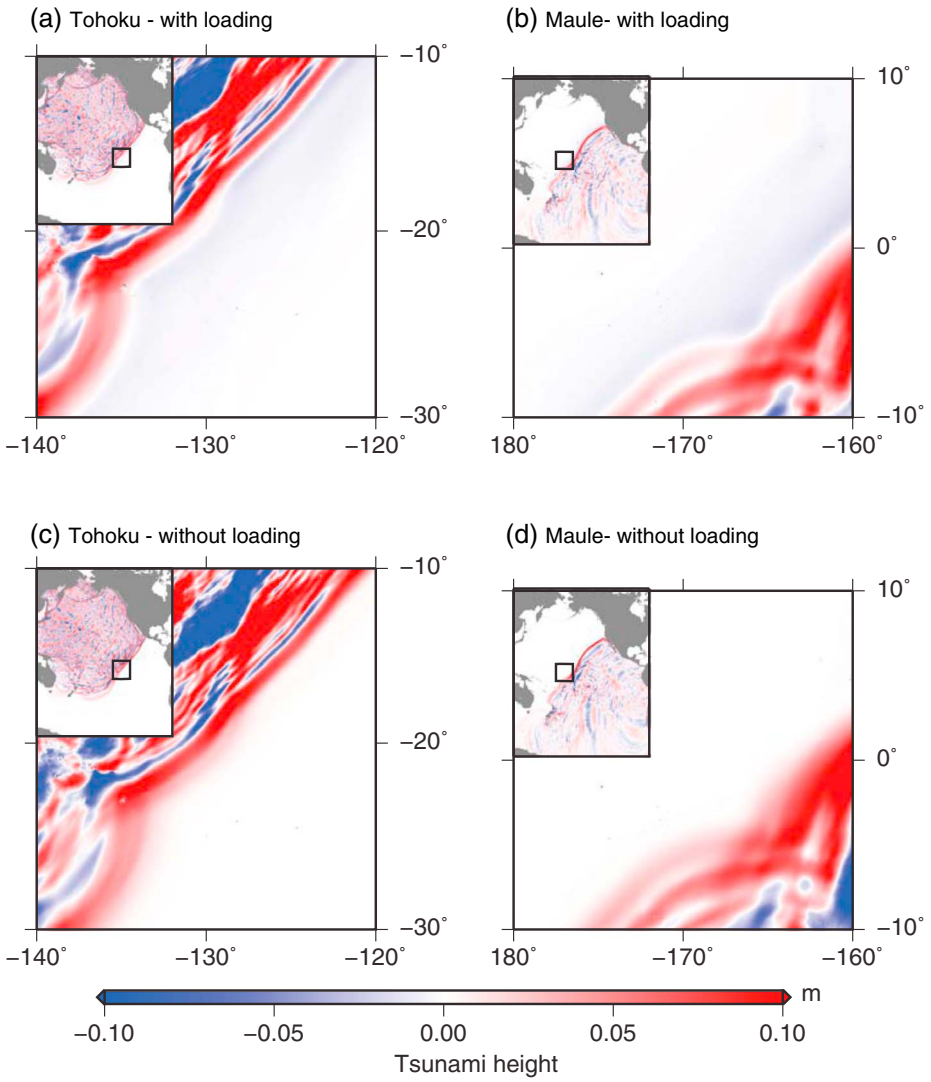

Figure 4. Comparison snapshots of the simulated tsunami wavefields at 14 h of propagation, (a and b) with and (c and d) without the loading effect.

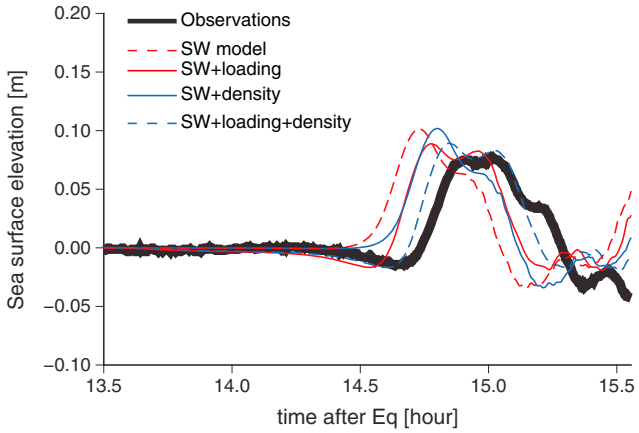

Figure 5. Comparison of the impact of the loading and density stratification effects for the tsunami waveform computed at DART51407 for the Maule tsunami, along with the observed data. We clearly observe that the density affects the time delay, but the loading causes both a time delay and a distortion of the waveform. Both effects need to be taken into account to have a better fit between observations and simulations.

near-nodal parts of the tsunami radiation pattern that might require a value for $\Delta\alpha$ (equation (9)) larger than the 800 km we used, or (4) some other as yet unknown and poorly modeled aspect of tsunami propagation.

7. Discussion and Conclusion

In this paper, we have augmented the classical description of tsunami propagation as a shallow water wave involving the motion of a constant-density fluid over a rigid substrate, with a description that accounts for the elastic response of the Earth to the tsunami mass load as well as density stratification of the water column. We have used an implementation of this new description to model two recent large tsunami events and showed that our new description substantially reduces the mismatch between observation and numerical simulations recognized in previous studies. We showed that the loading and stratification effects can correct the time delay and reproduce the small long-period negative phase that is often observed for tsunamis that have propagated over large distances.

In agreement with previous studies [*Tsai et al.*, 2013; *Watada*, 2013; *Inazu and Saito*, 2013], our results show that the effects of loading and stratification are not negligible, at least for studies in which the precise timing and waveform of the tsunami is a concern. While the effect on near-field tsunami waveforms (Figures 3a and 3e) is small, the arrival time discrepancies between simulations which include and do not include loading/stratification effects is 10–30 min for the far-field tsunami waveforms in Figures 3b–3e. As discussed above, these differences are large enough to affect tsunami source inversions using far-field data, so it will be necessary to use a physical description of tsunami propagation that accounts for elastic loading and density stratification if such data are to contribute to a better understanding of the tsunami source.

The extent of tsunami waveform distortion caused by the loading/stratification effect described here will depend on the characteristics of the source (e.g., the wavelength), as well as the particular ocean path traversed from source to receiver. These effects do not explain all discrepancies between observed and calculated tsunami waveforms reported in the literature, which can also be due to errors in bathymetry or source model. However, inclusion of the loading effect does allow a systematically reduced misfit for tsunami waveforms recorded at large distances, and so it should allow us to better use these data to identify and correct these additional sources of error.

Acknowledgments

This research was undertaken on the NCI National Facility on the Raijin-Fujitsu computing resource (project xc3) in Canberra, which is supported by the Australian Commonwealth Government. This research was supported by Australian Research Council Discovery Project (DP110101983) led by P. Cummins. Figures were made using the GMT-5 open source software. Data were processed using PYTHON. DART tsunami recordings were downloaded from the National Geophysical Data Center from the National Oceanic and Atmospheric Administration (NGDC–NOAA, NOAA). We thank Victor Tsai and an anonymous reviewer for their comments on the manuscript.

The Editor thanks Victor Tsai and an anonymous reviewer for their assistance in evaluating this paper.

References

Ammon, C. J., T. Lay, H. Kanamori, and M. Cleveland (2011), A rupture model of the 2011 off the Pacific coast of Tohoku earthquake, *Earth Planets Space*, *63*, 693–696, doi:10.5047/eps.2011.05.015.

Arakawa, A., and V. R. Lamb (1977), Computational design of the basic dynamical processes of the UCLA general circulation model, in *Methods of Computational Physics*, vol. 17, edited by J. Chang, pp. 173–265, Academic Press, New York.

Baba, T., P. Cummins, H. Thio, and H. Tsushima (2009), Validation and joint inversion of teleseismic waveforms for earthquake source models using deep ocean bottom pressure records: A case study of the 2006 Kuril megathrust earthquake, *Pure Appl. Geophys.*, *166*(1-2), 55–76, doi:10.1007/s00024-008-0438-1.

Boudin, F., et al. (2013), Analysis and modeling of tsunami-induced tilt for the 2007, M = 7.6, Tocopilla and the 2010, M = 8.8 Maule earthquakes, Chile, from long-base tiltmeter and broadband seismometer records, *Geophys. J. Int.*, *194*, 269–288, doi:10.1093/gji/ggt123.

Crank, J., and P. Nicolson (1947), A practical method for numerical evaluation of solutions of partial differential equations of the heat-conduction type, *Adv. Comput. Math.*, *6*, 207–226, doi:10.1007/BF02127704.

Farrell, W. E. (1972), Deformation of the Earth by surface loads, *Rev. Geophys.*, *10*(3), 761–797, doi:10.1029/RG010i003p00761.

Fujii, Y., and K. Satake (2012), Slip distribution and seismic moment of the 2010 and 1960 Chilean earthquakes inferred from tsunami waveforms and coastal geodetic data, *Pure Appl. Geophys.*, *170*(9-10), 1493–1509, doi:10.1007/s00024-012-0524-2.

Grilli, S. T., J. C. Harris, T. S. Tajalli Bakhsh, T. L. Masterlark, C. Kyriakopoulos, J. T. Kirby, and F. Shi (2012), Numerical simulation of the 2011 Tohoku tsunami based on a new transient FEM co-seismic source: Comparison to far- and near-field observations, *Pure Appl. Geophys.*, *170*(6-8), 1333–1359, doi:10.1007/s00024-012-0528-y.

Hendershott, M. C. (1972), The effects of solid Earth deformation on global ocean tides, *Geophys. J. R. Astron. Soc.*, *29*, 389–402, doi:10.1111/j.1365-246X.1972.tb06167.x.

IOC, IHO, and BODC (2003), Centenary edition of the GEBCO digital atlas, published on CD-ROM on behalf of the Intergovernmental Oceanographic Commission and the International Hydrographic Organization as part of the General Bathymetric Chart of the Oceans, British Oceanographic Data Centre, Liverpool, U. K.

Inazu, D., and T. Saito (2013), Simulation of distant tsunami propagation with a radial loading deformation effect, *Earth Planets Space*, *65*(8), 835–842, doi:10.5047/eps.2013.03.010.

Kirby, J. T., F. Shi, B. Tehranirad, J. C. Harris, and S. T. Grilli (2013), Dispersive tsunami waves in the ocean: Model equations and sensitivity to dispersion and Coriolis effects, *Ocean Modell.*, *62*, 39–55, doi:10.1016/j.ocemod.2012.11.009.

Lay, T., C. J. Ammon, H. Kanamori, K. D. Koper, O. Sufri, and A. R. Hutko (2010), Teleseismic inversion for rupture process of the 27 February 2010 Chile (M_W 8.8) earthquake, *Geophys. Res. Lett.*, *37*, L13301, doi:10.1029/2010GL043379.

Longman, I. M. (1962), A Green's function for determining the deformation of the Earth under surface mass loads: 1. Theory, *J. Geophys. Res.*, *67*(2), 845–850, doi:10.1029/JZ067i002p00845.

Lorito, S., F. Romano, S. Atzori, X. Tong, A. Avallone, J. McCloskey, M. Cocco, E. Boschi, and A. Piatanesi (2011), Limited overlap between the seismic gap and coseismic slip of the great 2010 Chile earthquake, *Nat. Geosci.*, *4*(3), 173–177, doi:10.1038/ngeo1073.

Nawa, K., N. Suda, K. Satake, Y. Fujii, T. Sato, K. Doi, M. Kanao, and K. Shibuya (2007), Loading and gravitational effects of the 2004 Indian Ocean tsunami at Syowa Station, Antarctica, *Bull. Seismol. Soc. Am.*, *97*(1A), S271, doi:10.1785/0120050625.

Okada, Y. (1985), Surface deformation due to shear and tensile faults in a half-space, *Bull. Seismol. Soc. Am.*, *75*(4), 1135–1154.

Okal, E. (2007), Seismic records of the 2004 Sumatra and other tsunamis: A quantitative study, *Pure Appl. Geophys.*, *164*(2-3), 325–353, doi:10.1007/s00024-006-0181-4.

Pagiatakis, S. D. (1990), The response of a realistic Earth to ocean tide loading, *Geophys. J. Int.*, *103*(2), 541–560, doi:10.1111/j.1365-246X.1990.tb01790.x.

Satake, K., Y. Fujii, T. Harada, and Y. Namegaya (2013), Time and space distribution of coseismic slip of the 2011 Tohoku earthquake as inferred from tsunami waveform data, *Bull. Seismol. Soc. Am.*, *103*(2B), 1473–1492, doi:10.1785/0120120122.

Tsai, V. C., J.-P. Ampuero, H. Kanamori, and D. J. Stevenson (2013), Estimating the effect of Earth elasticity and variable water density on tsunami speeds, *Geophys. Res. Lett.*, *40*, 492–496, doi:10.1002/grl.50147.

Watada, S. (2013), Tsunami speed variations in density-stratified compressible global oceans, *Geophys. Res. Lett.*, *40*, 4001–4006, doi:10.1002/grl.50785.